Distortional Lateral Torsional Buckling Analysis of Beams with Overhangs

Payam Pezeshky, Arash Sahraei, and Magdi Mohareb, M. ASCE

Abstract

The present study investigates the effect of web distortion on the lateral torsional buckling strength of Gerber systems. Towards this goal, a number of modifications are introduced into two finite element formulations for the distortional and non-distortional lateral torsional buckling analysis. The distortional formulation treats the web as a thin plate and the flanges as Gjelsvik members, and captures load height effects. The non-distortional formulation is based on the Vlasov beam kinematics and enables the enforcement of lateral restraints offset from the shear center while preserving the positive definiteness of the stiffness matrices. Both models are validated against shell finite element solutions and then utilized to develop moment gradient coefficients for Gerber beams, assess the web distortional effects, and quantify the influence of various lateral bracing scenarios, on the elastic lateral torsional buckling strength. Unlike rolled simply supported beams where web distortion is considered to be insignificant, the present study indicates that web distortion heavily influences the lateral torsional buckling strength of Gerber beams.

Keywords: Lateral torsional buckling, distortional buckling, beams with overhangs, load height, finite element, warping

This article is to be cited as:
Pezeshky P, Sahraei A, Mohareb M (2019) Distortional Lateral Torsional Buckling Analysis of Beams with Overhangs, Journal of Structural Engineering, 145(3) – 04018266

A copy-edited version of this article is available at
https://ascelibrary.org/doi/abs/10.1061/%28ASCE%29ST.1943-541X.0002271

[1] Research Associate, Dept. of Civil Engineering, University of Ottawa, Ottawa, ON, Canada. (Corresponding Author). Email: Payam.pezeshky@uottawa.ca

[2] Research Associate, Dept. of Civil Engineering, University of Ottawa, Ottawa, ON, Canada. Email: Asahr012@uottawa.ca

[3] Professor, Dept. of Civil Engineering, University of Ottawa, Ottawa, ON, Canada. Email: Mmohareb@uottawa.ca'

Introduction

The Gerber system (Fig. 1) consists of beams with overhangs connected to two adjacent suspended spans at the overhang tips. Typically, such beams have wide flange cross-sections and are thus prone to lateral torsional buckling (LTB). The Gerber system (Fig. 1) consists of a central span (or back-span) and two overhangs (cantilever spans). Traditionally, Gerber system spans are engineered so that the negative bending moments at the supports are nearly equal to the positive moments at the middle of the central span, with the intent to fully utilize the cross-sectional capacity in the regions of maximum positive and negative moments. Loads acting on Gerber systems arise from: (1) open web steel joists (OWSJ in Fig. 1) that frame perpendicularly to the beam axis, thus applying a series of point loads on the back-span and on the overhangs, and (2) the action of the suspended spans which give rise to point loads at the overhang tips. At the column location, the top and bottom chords of the OWSJ framing into the beam are typically connected to the Gerber beam flanges to provide lateral restraints (Fig. 1). At the connection between the end of the suspended span to the cantilever tip, the OWSJ framing into the cantilever tip provides lateral restraint either at the top flange alone (when connected to the beam top flange) or at both flanges (when both chords of the OWSJ are connected to the beam flanges). It is of interest to assess the effect of both bracing scenarios on the lateral torsional buckling capacity of Gerber systems, in a classical (non-distortional) sense and under a distortional lateral torsional buckling framework.

In classical lateral torsional buckling, the beam cross-section is assumed to displace laterally and twist as a rigid disk, thus omitting possible web distortion. Classical LTB solutions have been established in Barsoum and Gallagher (1970) and Trahair (1993). They form the basis of present

56 design provisions in structural steel standards for rolled members (e.g., CAN-CSA S16-16 (2016),
57 ANSI/AISC 360-16 (2016), EN-1993-1-1-05 (2005), AS/NZS 4600-05 (2005)) which presume
58 that web distortional effects are negligible. Recent studies suggest that web distortion can
59 influence the LTB strength of rolled steel members, including cantilevers (Pezeshky et al. (2017))
60 and simply supported beams with cleat angles (Hassan and Mohareb (2015)).

61 **Fig. 1.** Gerber beam system

62 Approximate distortional buckling solutions include the work of (Hancock (1978)) who developed
63 a finite strip solution and (Hancock et al. (1980)) who developed an energy-based approximate
64 solution. Wang et al. (1991) investigated the influence of web distortion on the LTB strength for
65 simply supported beams with mono-symmetric sections under uniform moments and extended
66 their work for beams under point loads (Hughes and Ma (1996a)) and distributed loads (Ma and
67 Hughes (1996b)). Samanta and Kumar (2006a) investigated the effect of web distortion on the
68 LTB of simply supported beams and cantilevers (Kumar and Samanta (2006b). Finite element
69 formulations for the problem include the work of Bradford and Trahair (1981) who developed a
70 12 degree of freedom (DOF) element, and (Bradford and Trahair (1982) and Chin et al. (1992))
71 who developed a 16 DOF element. A number of distortional buckling solutions were developed
72 for beams supported on seats (Bradford Mark and Trahair Nicholas (1983)), with mono-symmetric
73 sections (Bradford 1985,1988a), tee sections (Bradford 1988b, 1990a), beam-columns (Bradford
74 1990b and Vrcelj and Bradford 2006a), cantilevers (Bradford 1992a, 1999), and I-beams with
75 rotational and translational restraints (Bradford 1992b, Ronagh and Bradford 1994, and Bradford
76 and Ronagh 1997). A distortional buckling finite element by Ng and Ronagh (2004) adopted cubic
77 polynomials to characterize the variation of the lateral displacement along the section depth and
78 sinusoidal functions in the longitudinal direction. A distortional model by Dekker and Kemp

(1998) adopted continuous springs between the top and bottom flanges to characterize web distortion. Pi and Trahair (2000) introduced the effective torsional constant concept to characterize distortional critical moments and investigated the effects of warping rigidity provided by end supports. Experimental studies in (Zirakian and Showkati (2006)) investigated the distortional LTB of castellated I-beams. Also, Zirakian and Showkati (2007) investigated the distortional effects in simply supported I-beams with mid-span concentrated loads. Using 3D shell models in Abaqus, Samanta and Kumar (2008) investigated the effect of lateral bracing and load height effects on the distortional LTB of cantilevers. The Generalized Beam Theory (GBT) methodology has also been adopted to develop distortional buckling models (e.g., Basaglia and Camotim (2013), de Miranda et al. (2013) and Vieira et al. (2017)). Pezeshky and Mohareb (2014) developed a distortional theory for the static analysis of mono-symmetric beams and formulated finite element solutions (Pezeshky and Mohareb (2015)).

Within the above context, the present study introduces modifications and adds new features to past distortional and non-distortional LTB finite element formulations and then adopts the modified solutions to investigate the LTB behavior of Gerber beams.

Statement of the problem

A doubly symmetric wide flange steel section (Fig. 2a) is subjected to a general transverse line load $q_z(x)$ (Fig. 2b) acting at a load height $z_q(x)$. The beam is assumed to be laterally restrained only at selected discrete points at the top and/or bottom flanges. It is required to determine the critical load $\lambda q_z(x)$ at which the beam has a tendency to buckle either in a distortional lateral torsional buckling mode, or in a non-distortional mode (Fig. 3). Towards this goal, modifications and new features are introduced into the distortional the elements of Bradford and Trahair (1982)

and the non-distortional element by Barsoum and Gallagher (1970). The modified models are subsequently used to assess the LTB strength of Gerber systems.

Assumed Kinematics

A right-handed coordinate system (Fig. 2a) is adopted in which origin 'O' lies on web mid-height. A local right-handed coordinate system is also assigned to each of the flanges and to the web. Points A, B and C within the top flange, bottom flange, and the web are respectively offset from the middle surface and have local coordinates (y, n_F), (y, n_F) and (z, n). The un-deformed beam is shown in Configuration 1 in Fig. 3. Under the reference load $q_z(x)$, the beam moves to Configuration 2 by undergoing transverse displacement $w(x)$. During the pre-buckling deformation stage (Configuration 1 to 2), transverse response $w(x)$ of the beam is assumed to follow that of the conventional Euler beam theory. The pre-buckling analysis yields the internal forces (moments, shears, and associated stresses) needed to conduct the buckling analysis. The load is then assumed to increase to $\lambda q_z(x)$ and the beam moves to Configuration 3 at the onset of buckling. Assuming a linear force-displacement relationship, the transverse displacement of the beam increased to $\lambda w(x)$. The beam then buckles under no increase in loading by displacing laterally from Configuration 3 to Configuration 4.

For the case of distortional buckling, Configuration 4 is characterized by the lateral displacement $v(x,z)$ where the web is assumed to act as a thin plate, while the flanges are assumed to act as a Gjelsvik thin-walled members (Gjelsvik (1981)) under compression (Fig. 3). The top flange displaces laterally through $v_T(x) = v(x, h/2)$ and twists through $\theta_T(x) = -v_{,z}(x,z)_{z=h/2}$ while the bottom flange displaces laterally through $v_B(x) = v(x, -h/2)$ and twists through

$\theta_B(x) = -v_{,z}(x,z)_{z=-h/2}$. As a matter of convention ',' denotes partial differentiation with respect to the argument coordinate. Also, all fields with subscript '' denote variables pertaining to the top flange and those with subscript ' B ' pertain to the bottom flange.

For the case of classical non-distortional buckling, the section is assumed to displace as rigid disk and Configuration 4 is characterized by a lateral displacement $v_0(x)$ at the section shear center and an angle of twist $\theta(x)$. Under both distortional and non-distortional buckling analyses, it is required to determine the load multiplier λ at which the system will buckle.

Pre-buckling Analysis

The conventional two-node Euler Bernoulli beam element is used to extract the nodal shear forces and bending moments V_1, M_1, V_2, and M_2 at member ends. Linear interpolation is used to approximate the shear forces and bending moments at Configuration 3, i.e.,

$$\lambda M_y(x) = \lambda M_1\left(1-\frac{x}{L}\right) - \lambda M_2\left(\frac{x}{L}\right), \quad \lambda V(x) = \lambda V_1\left(1-\frac{x}{L}\right) - \lambda V_2\left(\frac{x}{L}\right) \tag{1}$$

where the positive sign conventions for the shear force $V(x)$ and bending moment $M(x)$ are shown in Fig. 4. The corresponding normal and shearing stresses as given by the beam theory are

$$\lambda\sigma_x(x,z) = -\lambda\frac{M_y(x)}{I_y}z\ , \qquad \lambda\tau_{xz}(x,z) = \frac{\lambda V(x)Q_y(z)}{I_y t_w} \tag{2}\text{a-b}$$

and the negative sign in Eq. (2)a ensures that positive moments (Fig. 4) induce compressive stresses at the top flange $z = +h/2$, I_y is the major moment of inertia, h is the section height, and $Q_y(z)$ is the corresponding first moment of inertia about the y axis given by

$$.Q_y(z) = \left(bt\frac{h}{2}\right) + t_w\left(\frac{h-t}{2}-z\right)\left(z+\frac{h-t}{4}\right). \tag{3}$$

For the flanges, the contribution of the shear stresses is assumed negligible i.e., $\tau_{xz}(x,z) \approx 0$ compared to those in the web.

Fig. 2. a) Cross section geometry b) general type of loads

Fig. 3. Deformation stages of buckling

The normal stresses at top flange $\sigma_{xT}(x, z = h/2) = -(h/2)M(x)/I_y$ and bottom flange $\sigma_{xB}(x, z = -h/2) = (h/2)M(x)/I_y$ are obtained by setting the z coordinate as $z = +h/2, -h/2$, respectively. From Eqs. (1) and (3) by substituting into Eqs. (2)a-b, one obtains the normal and shear stresses within the web, i.e.

$$\lambda\sigma_x(x,z) = -\frac{\lambda M(x)}{I_y} z = \lambda \frac{1}{I_y}\left[M_1\left(1-\frac{x}{L}\right) - M_2\left(\frac{x}{L}\right)\right] z \qquad -\frac{h}{2} \le z \le \frac{h}{2}$$

$$\lambda\tau_{xz}(x,z) = \frac{\lambda V(x) Q_y(z)}{I_y t_w} = \frac{\lambda}{I_y t_w}\left[bt + t_w\left(\frac{h-t}{2} - z\right)\left(z + \frac{h-t}{4}\right)\right]\left[V_1\left(1-\frac{x}{L}\right) - V_2\left(\frac{x}{L}\right)\right]$$

(4)a-b

Fig. 4. Sign convention for stress resultants

Distortional Buckling Analysis

Overview of relevant past work

Bradford and Trahair (1982) developed a distortional lateral torsional buckling element for mono-symmetric thin-walled beams with a flexible web and two symmetric flange assemblies, each consisting of folded plates. When developing the underlying variational expression, the Bradford and Trahair element (subsequently referred to as BT) treats the web as a thin plate. To account for the flexibility of the web, the study assumed the lateral displacements of the web to follow a cubic distribution along the height, while treating each of the flange assemblies as Vlasov beams, hence capturing their global warping behavior.

The present Distortional formulation (subsequently referred as D solution) tackles doubly symmetric I-sections. In a manner identical to BT solution, the D solution treats the web as a thin plate with a cubic distribution for the lateral displacement. In contrast to the BT solution, it treats the flanges as Gjelsvik members (thus accounts for their local warping effects) subjected to longitudinal stresses. Additional features of the present D solution are that it captures (1) the quadratic distribution of the shear stresses along the web height (as opposed to a constant shear stress in the BT solution) and (2) the destabilizing effect due to load height, a feature not supported in past distortional lateral torsional buckling beam formulation.

Modified Variational Formulation

The total potential energy Π in going from Configuration 3 to 4 is summation of $\Pi = \Pi_W + \Pi_T + \Pi_B + V$ where Π_W , Π_T and Π_B are the total potential energies within the web, top and bottom flanges and V is the load potential increase of loads undergoing vertical displacements due to the twist of the section. The web is treated as a thin plate as discussed under the section on kinematic assumptions. The total potential energy Π_W for the web, as given in (e.g., Timoshenko and Woinowsky-Krieger (1956), Bradford and Trahair 1982), is

$$\Pi_W = \int_0^L \int_{-h/2}^{h/2} \left\{ \frac{D}{2}\left[\left(v_{,xx}\right)^2 + \left(v_{,zz}\right)^2 + 2\mu v_{,xx} v_{b,zz} + 2\left(1-\mu\right)\left(v_{,xz}\right)^2 \right] + \frac{\lambda}{2}\left[t_w \sigma_x v^2{}_{,x} + 2 t_w \tau_{xz} v_{,x} v_{,z} \right] \right\} dz dx \tag{5}$$

where $D = Et_w^3/12(1-\nu^2)$ is the flexural rigidity of the plate, E is Young modulus, μ is Poisson's ratio, and $\lambda\sigma_x\left(x,z\right), \lambda\tau_{xz}\left(x,z\right)$ are the normal and shear stresses in the plate. The first integral in Eq. (5) is the internal strain energy due to bending of the web and the second term is the destabilizing term due to internal normal stress σ_x and shear stress τ_{xz}.

As mentioned under the kinematic assumptions, the flanges are considered to behave a Gjelsvik beams under axial stresses. Throughout buckling, the flanges undergo lateral bending and twist. Hence the total potential energy terms Π_T, Π_B of the top and bottom flanges are expressed as

$$\Pi_T = \frac{1}{2}\int_0^L \left(EI_{zzF} v_{,xx}^2 + EI_{wwF} v_{,xxz}^2 + GJ_F v_{,xz}^2 \right)_{(y=h/2)} dx + \frac{\lambda}{2}\int_0^L \left[\sigma_{xT}\left(x, z=h/2\right)\left(I_{pF} v_{,xz}^2 + A_F v_{,x}^2 \right) \right]_{(z=h/2)} dx \tag{6}$$

$$\Pi_B = \frac{1}{2}\int_0^L \left(EI_{zzF} v_{,xx}^2 + EI_{wwF} v_{,xxz}^2 + GJ_F v_{,xz}^2 \right)_{(y=-h/2)} dx + \frac{\lambda}{2}\int_0^L \left[\sigma_{xB}\left(x, z=-h/2\right)\left(I_{pF} v_{,xz}^2 + A_F v_{,x}^2 \right) \right]_{(z=-h/2)} dx \tag{7}$$

where G is the shear modulus, and relevant sectional properties for the flanges are

$$\left(A_F, I_{zzF}, I_{pF}, J_F, I_{wwF} \right) = \int_{A_F} \left(1, y^2, y^2 + n_F^2, 4n_F^2, n_F^2 y^2 \right) dA_F = \left(bt, b^3 t/12, \left(b^3 t + bt^3 \right)/12, bt^3/3, b^3 t^3/144 \right)$$

where n_F is the normal local coordinate for the flanges (Fig. 2a), A_F is the cross sectional area, I_{zzF} is the strong axis moment of inertia, I_{pF} is the polar moment of inertia, J_F is the Saint-Venant torsional constant and I_{wwF} is the local warping constant, all defined for a single flange.

The reference line load $q_z(x)$ is applied at a height $z_q(x)$ above the shear center (Fig. 2). Throughout buckling (i.e., in deforming from Configuration 3 to 4), load $q_z(x)$ undergoes a vertical displacement $w_b(x)$ (Fig. 5b) and the corresponding total potential gain is obtained by the product of load increment $q_z(x)dx$ and the displacement $w_b(x) = -\frac{1}{2}\int_{z=0}^{z_q(x)} \left[v_{,z}(x,z) \right]^2 dz$. Integrating with respect to x one recovers the total load potential energy gain as

$$V = \lambda \int_0^L q_z(x) w_b(x) dx = -\frac{\lambda}{2}\int_0^L q_z(x) \int_{z=0}^{z_q(x)} \left[v_{,z}(x,z) \right]^2 dz dx \tag{8}$$

Fig. 5. Vertical distance travelled by load throughout buckling

In summary, by adding the total potential energy of the web Π_W Eq. (5), flanges Π_T and Π_B Eqs. (6)-(7) and load potential due to external loads V Eq. (8) one recovers the total potential energy as

$$\Pi = \int_0^L \int_{-h/2}^{h/2} \left\{ \frac{D}{2} \left[\left(v_{,xx}\right)^2 + \left(v_{,zz}\right)^2 + 2\mu v_{,xx} v_{b,zz} + 2\left(1-\mu\right)\left(v_{,xz}\right)^2 \right] + \frac{\lambda}{2} \left[t_w \sigma_x v^2{}_{,x} + 2 t_w \tau_{xz} v_{,x} v_{,z} \right] \right\} dxdz$$

$$+ \frac{1}{2} \int_0^L \left\{ \left(EI_{zzF} v^2_{,xx} + EI_{wwF} v^2_{,xxz} + GJ_F v^2_{,xz} \right) + \lambda \left[\sigma_{xT} \left(x, z = h/2 \right) \left(I_{pF} v^2_{,xz} + A_F v^2_{,x} \right) \right] \right\}_{(z=h/2)} dx$$

$$+ \frac{1}{2} \int_0^L \left\{ \left(EI_{zzF} v^2_{,xx} + EI_{wwF} v^2_{,xxz} + GJ_F v^2_{,xz} \right) + \lambda \left[\sigma_{xB} \left(x, z = -h/2 \right) \left(I_{pF} v^2_{,xz} + A_F v^2_{,x} \right) \right] \right\}_{(z=-h/2)} dx$$

$$- \frac{\lambda}{2} \int_0^L q_z \left(x\right) \int_{z=0}^{z_q(x)} \left(v_{,z}\right)^2 dzdx \qquad (9)$$

Finite Element Formulation

A finite element with four nodes $j = 1, 2, 3, 4$ with 4 degrees of freedom (DOFs) per node is developed (Fig. 6) for the buckling analysis. The four degrees of freedom of node j are the lateral displacement v_j, the rotation $\left(v_{,x}\right)_j$, the angle of twist θ_j and the rate of change of the angle of twist $\left(\theta_{,x}\right)_j$ with respect to the longitudinal coordinate.

Fig. 6. Definition of the 16 DOFs in the distortional buckling element

Contribution of the web

The displacement field $v\left(x,z\right)$ for the web can be expressed in terms of the nodal displacements of the element through cubic Hermitian polynomials in both directions, i.e.,

$$v\left(x,z\right) = \mathbf{M}^{\mathbf{T}}_{\mathbf{1\times 16}}\left(x,z\right)\mathbf{u}_{\mathbf{b(16\times 1)}} \qquad (10)$$

where $\mathbf{M}\left(x,y\right)$ is the vector of shape functions resulting from the product of Hermitian functions in both directions, i.e.,

$$\mathbf{M}^{\mathbf{T}}_{\mathbf{1\times 16}}\left(x,z\right) = \left\langle H_1\left(z\right)\bar{\mathbf{N}}^{\mathbf{T}}\left(x\right) \mid H_2\left(z\right)\mathbf{N}^{\mathbf{T}}\left(x\right) \mid H_3\left(z\right)\bar{\mathbf{N}}^{\mathbf{T}}\left(x\right) \mid H_4\left(z\right)\mathbf{N}^{\mathbf{T}}\left(x\right) \right\rangle_{\mathbf{1\times 16}} \qquad (11)$$

and the shape functions $H_1\left(z\right) - H_4\left(z\right)$ and $\mathbf{N}_{\mathbf{1\times 4}}\left(x\right)$ are given by

219 $$H_1(z)=\frac{1}{2}+\frac{3z}{2h}-\frac{2z^3}{h^3}\ , \qquad H_2(z)=-\frac{h}{8}-\frac{z}{4}+\frac{z^2}{2h}+\frac{z^3}{h^2}$$
$$H_3(z)=\frac{1}{2}-\frac{3z}{2h}+\frac{2z^3}{h^3}, \qquad H_4(z)=\frac{h}{8}-\frac{z}{4}-\frac{z^2}{2h}+\frac{z^3}{h^2} \qquad (12)$$

220 and $$\mathbf{N}(x)^{\mathbf{T}}_{\mathbf{1\times 4}}=\left\langle 1-3\left(\frac{x}{L}\right)^2+2\left(\frac{x}{L}\right)^3 \;\middle|\; x-\left(2\frac{x^2}{L}\right)+\left(\frac{x^3}{L^2}\right) \;\middle|\; 3\left(\frac{x}{L}\right)^2-2\left(\frac{x}{L}\right)^3 \;\middle|\; \frac{x^3}{L^2}-\frac{x^2}{L}\right\rangle$$

221 $$\bar{\mathbf{N}}(x)^{\mathbf{T}}_{\mathbf{1\times 4}}=\left\langle 1-3\left(\frac{x}{L}\right)^2+2\left(\frac{x}{L}\right)^3 \;\middle|\; -x+\left(2\frac{x^2}{L}\right)-\left(\frac{x^3}{L^2}\right) \;\middle|\; 3\left(\frac{x}{L}\right)^2-2\left(\frac{x}{L}\right)^3 \;\middle|\; -\frac{x^3}{L^2}+\frac{x^2}{L}\right\rangle \qquad (13)\text{a-b}$$

222 in which $-h/2\le z\le h/2$, $0\le x\le L$. In Eq. (10), vector $\mathbf{u}^{\mathbf{T}}_{\mathbf{b(1\times 16)}}=\left\langle \mathbf{u}^{\mathbf{T}}_{\mathbf{b1}} \quad \mathbf{u}^{\mathbf{T}}_{\mathbf{b2}} \quad \mathbf{u}^{\mathbf{T}}_{\mathbf{b3}} \quad \mathbf{u}^{\mathbf{T}}_{\mathbf{b4}} \right\rangle$ contains

223 the nodal displacements vectors defined as

224 $$\left(\mathbf{u}^{\mathbf{T}}_{\mathbf{b1}},\mathbf{u}^{\mathbf{T}}_{\mathbf{b2}},\mathbf{u}^{\mathbf{T}}_{\mathbf{b3}},\mathbf{u}^{\mathbf{T}}_{\mathbf{b4}}\right)=\left(\left\langle v_1 \quad v_{,x1} \quad v_3 \quad v_{,x3}\right\rangle,\left\langle \theta_1 \quad \theta_{,x1} \quad \theta_3 \quad \theta_{,x3}\right\rangle,\left\langle v_2 \quad v_{,x2} \quad v_4 \quad v_{,x4}\right\rangle,\left\langle \theta_2 \quad \theta_{,x2} \quad \theta_4 \quad \theta_{,x4}\right\rangle\right)$$

225 and the interpolation functions $\mathbf{M}(x,z)$ appearing in Eq. (10) relate the lateral displacement of the web

226 to the nodal displacements $\mathbf{u}_{\mathbf{b}k}$ through $v(x,z)=\sum_{k=1}^{16}\mathbf{M}_k(x,z)\mathbf{u}_{\mathbf{b}k}$. From Eq. (10), by substituting into

227 Eq. (5), one can express the total potential energy for the web as

228 $$\Pi_W=\frac{1}{2}\mathbf{u}^{\mathbf{T}}_{\mathbf{b}}\left[\left(\mathbf{k_1}+\mathbf{k_2}+\mathbf{k_3}+\mathbf{k_4}\right)+\lambda\left(\mathbf{k_{1g}}+\mathbf{k_{2g}}\right)\right]\mathbf{u_b} \qquad (14)$$

229 where the elastic matrices $\mathbf{k_1}-\mathbf{k}_4$ and geometric matrices $\mathbf{k_{1g}},\mathbf{k_{2g}}$ are defined as

230 $$\left[\mathbf{k_1},\mathbf{k}_2,\mathbf{k}_3,\mathbf{k}_4\right]=D\int_0^L\int_{-h/2}^{h/2}\left[\mathbf{M_{,xx}M^{T}_{,xx}},\mathbf{M_{,zz}M^{T}_{,zz}},2\mu\mathbf{M_{,xx}M^{T}_{,zz}},2(1-\mu)\mathbf{M_{,xz}M^{T}_{,xz}}\right]dzdx$$

231 $$\left(\mathbf{k}_{1g},\mathbf{k}_{2g}\right)=\int_0^L\int_{-h/2}^{h/2}\left(N_x\mathbf{M_{,x}M^{T}_{,x}},N_{xz}\mathbf{M_{,x}M^{T}_{,z}}\right)dzdx$$

232 where, $N_x=t_w\sigma_x$ and $N_{xz}=2t_w\tau_{xz}$.

Contributions of the flange:

In order to express the total potential energy of the flange, the field displacement v is obtained at the top flange by setting $z = h/2$ in the shape functions (i.e., $\mathbf{M}_k\left(x, h/2\right)$). From Eq. (10) by substituting into Eq. (6), one rewrites the total potential energy of the top flange as

$$\Pi_T = \frac{1}{2}\mathbf{u_b^T}\left[\left(\mathbf{k_5} + \mathbf{k_6} + \mathbf{k_7}\right) + \lambda\left(\mathbf{k_{3g}} + \mathbf{k_{4g}}\right)\right]_{(z=h/2)}\mathbf{u_b} \tag{15}$$

where the elastic matrices $\mathbf{k_5}$ - $\mathbf{k_7}$ and geometric matrices $\mathbf{k_{3g}}$ - $\mathbf{k_{4g}}$ are defined as

$$\begin{aligned}\left(\mathbf{k}_5, \mathbf{k}_6, \mathbf{k}_7\right) &= E\int_0^L \left(I_{zz}\mathbf{M}_{,\mathbf{xx}}\mathbf{M}_{,\mathbf{xx}}^{\mathbf{T}}, I_{\omega\omega}\mathbf{M}_{,\mathbf{xxz}}\mathbf{M}_{,\mathbf{xxz}}^{\mathbf{T}}, \left(GJ/E\right)\mathbf{M}_{,\mathbf{xz}}\mathbf{M}_{,\mathbf{zz}}^{\mathbf{T}}\right)_{(z=h/2)} dzdx \\ \left(\mathbf{k}_{3g}, \mathbf{k}_{4g}\right) &= \int_0^L \int_{-h/2}^{h/2} \left(I_{pF}\sigma_{xT}\left(x, z = h/2\right)\mathbf{M}_{,\mathbf{xz}}\mathbf{M}_{,\mathbf{xz}}^{\mathbf{T}}, A_F\sigma_{xT}\left(x, z = h/2\right)\mathbf{M}_{,\mathbf{x}}\mathbf{M}_{,\mathbf{x}}^{\mathbf{T}}\right) dzdx\end{aligned}$$

Analogous expressions can be obtained for the bottom flange by replacing subscript ' T 'with' B ' and setting $z = -h/2$ instead of $z = h/2$ in Eqs. (15), leading to $\Pi_B = \frac{1}{2}\mathbf{u_b^T}\left[\left(\mathbf{k_8} + \mathbf{k_9} + \mathbf{k_{10}}\right) + \lambda\left(\mathbf{k_{5g}} + \mathbf{k_{6g}}\right)\right]_{(z=-h/2)}\mathbf{u_b}$, where the elastic matrices $\mathbf{k_8}$ - $\mathbf{k_{10}}$ and geometric matrices $\mathbf{k_{5g}}$ - $\mathbf{k_{6g}}$ relate to the bottom flange.

Geometric stiffness matrix due to load height effect

From Eq. (10) by substituting into Eq.(8), the load potential energy at Stage 4 (i.e. buckling configuration) is expressed in terms of nodal displacement as

$$V = \frac{1}{2}\lambda\mathbf{u_b^T}\mathbf{K}_{g7}\mathbf{u_b} \tag{16}$$

where the geometric matrix $\mathbf{K}_{g7}$ is defined by $\mathbf{K}_{g7} = -\int_0^L q_z\left(x\right)\int_{z=0}^{z_q(x)}\mathbf{M}_{,\mathbf{z}}\mathbf{M}_{,\mathbf{z}}^{\mathbf{T}} dzdx$

Stationary condition

The stationary condition is evoked by setting the variation of total potential energy to zero, i.e.,

$$\delta\Pi = \delta\left(\Pi_W + \Pi_T + \Pi_B + V\right) = 0 \tag{17}$$

From Eqs. (14)-(16), by substituting into Eq. (17) and taking the variation with respect to the nodal displacements, one recovers the eigenvalue problem such as $\delta\Pi = \delta\mathbf{u}_\mathbf{b}^\mathbf{T}\left[\sum_{i=1}^{10}\mathbf{k}_i + \lambda\sum_{j=1}^{7}\mathbf{k}_{j,g}\right]\mathbf{u}_\mathbf{b} = 0$

Non-distortional Solution

Overview of relevant past work

The literature on non-distortional beam buckling solutions is vast. Most notable is the classical finite element by Barsoum and Ghallagher (1970). More recent developments include the work of Erkmen and Mohareb (2006a), Erkmen and Mohareb (2006b),Wu and Mohareb (2011a) and Wu and Mohareb (2011b). For comprehensive reviews on the subject, the interested reader is referred to the recent reviews in Sahraei and Mohareb (2016) and Sahraei et al. (2018). The proposed non-distortional solution herein is based on a modification of the element of (Barsoum and Gallagher 1970). The element as originally formulated is based on the lateral displacement of the shear center and the angle of twist and is thus able to naturally model lateral braces at the shear center and twisting braces. In its original form, it cannot directly model lateral restraints at the top or bottom flanges. This feature is added in the present work. The total potential energy in going from the point of onset of buckling to the buckled configuration is

$$\Pi_{eb} = \left(U_v + U_{sv} + U_w\right) + V_b \tag{18}$$

where U_v , U_{sv}, U_w are the internal strain energy stored due to weak axis bending, conventional Saint-Venant torsion, and warping torsion, respectively. Also, the destabilizing load potential energy terms $V_b = V_m + V_{qL}$ consists of a component V_m due to the bending moments and another one V_{qL} due to load position effect. By expressing the above energy terms in terms of the lateral displacement v and the angle of twist θ, one obtains

$$\left[U_v, U_{sv}, U_w, V_m, V_{qL}\right] = \frac{1}{2}\int_0^L \left[EI_z v_{,xx}^2, GJ\theta_{,x}{}^2, EC_w\theta_{,xx}{}^2, \lambda M_y(x)\theta\, v_{,xx}, \lambda q(x) z_q \theta^2\right] dx \qquad (19)$$

in which, J is the Saint-Venant torsional constant, I_z is the moment of inertia of the section about z-axis, and C_w is the warping constant of the section. The finite element has two nodes, each having four buckling degrees of freedom; the lateral displacement v, the weak-axis rotation $v_{,x}$, the angle of twist θ and the warping deformation $\theta_{,x}$. The lateral displacement v is related to the nodal displacements and rotations $\mathbf{v}^{\mathrm{T}} = \langle v_1 \quad v_{,x1} \quad v_2 \quad v_{,x2} \rangle$ and the angle of twist θ are related in terms of nodal rotations and warping deformation $\boldsymbol{\theta}^T = \langle \theta_1 \quad \theta_{,x1} \quad \theta_2 \quad \theta_{,x2} \rangle$ using Hermitian polynomials as

$$v(x) = \bar{\mathbf{N}}(x)_{1\times 4}^T \mathbf{v}_{4\times 1}, \quad \theta(x) = \mathbf{N}(x)_{1\times 4}^T \boldsymbol{\theta}_{4\times 1} \qquad (20)\text{a-b}$$

where $\mathbf{N}(x)$ and $\bar{\mathbf{N}}(x)$ have been defined in Eq. (13)a-b. From Eqs. (19), (20)a-b, by substituting into Eq. (18) one recovers

$$\Pi_{eb} = \left(\frac{1}{2}\right) \mathbf{u}_{\mathbf{b}1\times 8}^{\mathbf{T}} \left[\mathbf{k}_{\mathbf{E}8\times 8} - \lambda \mathbf{k}_{\mathbf{G}8\times 8}\right] \mathbf{u}_{\mathbf{b}8\times 1} \qquad (21)$$

where $\mathbf{k_E}$ is the elastic stiffness matrix, and $\mathbf{k_G}$ is the geometric stiffness matrix and the corresponding nodal displacement vector is $\mathbf{u_b^T} = \langle (v \quad \theta \quad v_{,x} \quad \theta_{,x})_1 \,\vdots\, (v \quad \theta \quad v_{,x} \quad \theta_{,x})_2 \rangle$. The above element based on the displacement vector $\mathbf{u_b^T}$ allows the modelling of braces at the section shear center and will be referred to as the "BG element" subsequently.

Modifications to previous work

In the BG element, the nodal lateral displacements $v_i\,(i = 1, 2)$ in vector $\mathbf{u_b^T}$ are defined at the shear center and θ_i are the angles of twist of the cross-section. In situations where one of the flanges is

laterally restrained while the other is non-restrained (Fig. 7a), rather than characterizing the motion of the cross-section using nodal displacements v_i and θ_i, it becomes more convenient to adopt the displacements of the top and bottom flanges v_{Ti} and v_{Bi} instead. The lateral displacements of the top and bottom flanges are related to the shear center lateral displacement and angle of twist of the section (Fig. 7b) through the relations $v_{Ti,B_i} = v_i \mp (h/2)\theta_i$. When a lateral brace is provided, for example at the top flange, one can express the kinematic constraint $v_{T1} = 0$. Such a constraint can be enforced, for example, using Lagrange multipliers (Sahraei and Mohareb (2016)). However, the process increases the size of the structure stiffness matrix and the resulting stiffness matrix loses its positive definite character, both aspects being undesirable in commercial software. Thus, a technique is developed herein to preserve the positive definite nature of the structure stiffness matrix. Three cases of practical interest (Fig. 7c) may arise. These are:

Case 1 –Both ends of the element have braces at one of (or both) flanges. In this case, the element needs to be developed in terms of the top and bottom flanges displacements at both nodes and the nodal displacement vector would be $\mathbf{u}_{\mathbf{b1}}^{\mathbf{T}} = \left\langle \mathbf{u}_{\mathbf{m1,1}}^{\mathbf{T}} \;\middle|\; \mathbf{u}_{\mathbf{m1,2}}^{\mathbf{T}} \right\rangle = \left\langle \left(v_T \quad v_{,xT} \quad v_B \quad v_{,xB} \right)_1 \;\middle|\; \left(v_T \quad v_{,xT} \quad v_B \quad v_{,xB} \right)_2 \right\rangle$. The resulting element will be termed as the BG1 element and the corresponding stiffness and geometric matrices will be developed subsequently.

Case 2- The first end of the element is braced at the shear center and the other end of the element is braced at one of the flanges (Fig. 7c-BG2). In such a case, the element matrices need to be formulated in terms of the nodal displacements $\mathbf{u}_{\mathbf{b2}}^{\mathbf{T}} = \left\langle \left(v \quad \theta \quad v_{,x} \quad \theta_{,x} \right)_1 \;\middle|\; \left(v_T \quad v_{,xT} \quad v_B \quad v_{,xB} \right)_2 \right\rangle$. Such an element can serve as a transition element between a BG zone of elements and another BG1 zone of elements (Fig. 7a) and will be referred to as the BG2 element.

Case 3- The first end of the element is braced at one of the flanges and the other end of the element is braced at the shear center (Fig. 7c-BG3). In such a case, the element matrices need to be formulated in terms of nodal displacements $\mathbf{u}_{\mathbf{b3}}^{\mathbf{T}} = \left\langle \left(v_T \quad v_{,xT} \quad v_B \quad v_{,xB} \right)_1 \;\vdots\; \left(v \quad \theta \quad v_{,x} \quad \theta_{,x} \right)_2 \right\rangle$. The element can serve as a transition element between a BG1 zone of element and another BG zone of elements (Fig. 7a). It is noted that in a zone of no lateral braces, no displacement constraints need to be imposed, and any of the elements BG, BG1, BG2, and BG3 can be used to model to the segment. For all three elements BG1, BG2, or BG3, the nodal displacement vector $\mathbf{u}_{\mathbf{bi}}^{\mathbf{T}} (i = 1 \equiv \text{BG1}, 2 \equiv \text{BG2}, 3 \equiv \text{BG3})$ can be related to the displacements $\mathbf{u}_{\mathbf{b}}$ through

$$\mathbf{u}_{\mathbf{b}8\times1} = \mathbf{A}_{\mathbf{i}8\times8} \mathbf{u}_{\mathbf{bi}8\times1} \tag{22}$$

where $\mathbf{A}_i$ is a transformation matrix depending on the section height h given in the following section. From Eq. (22), by substituting into Eq. (21), the total potential energy Π_{eb} takes the form

$$\Pi_{eb} = \frac{1}{2} \mathbf{u_b}^{\mathbf{T}} \left[\mathbf{k_E} - \lambda \mathbf{k_G} \right] \mathbf{u_b} = \frac{1}{2} \mathbf{u_{bi}}^{\mathbf{T}} \mathbf{A_i}^{\mathbf{T}} \left[\mathbf{k_E} - \lambda \mathbf{k_G} \right] \mathbf{A_i} \mathbf{u_{bi}} = \frac{1}{2} \mathbf{u_{bi}}^{\mathbf{T}} \left[\mathbf{k_{Ei}} - \lambda \mathbf{k_{Gi}} \right] \mathbf{u_{bi}} \tag{23}$$

where the modified elastic and geometric matrices $\mathbf{k_{Ei}}$ and $\mathbf{k_{Gi}}$ are given by

$$\mathbf{k_{Ei}} = \mathbf{A_i}^{\mathbf{T}} \mathbf{k_E} \mathbf{A_i}, \quad \mathbf{k_{Gi}} = \mathbf{A_i}^{\mathbf{T}} \mathbf{k_G} \mathbf{A_i}$$

Transformation matrices

Case 1:

For the first node, one can write $v_{T1} = v_1 - (h/2)\theta_1$, $v_{B1} = v_1 + (h/2)\theta_1$, $v_{,xT1} = v_{,x1} - (h/2)\theta_{,x1}$ and $v_{,xB1} = v_{,x1} + (h/2)\theta_{,x1}$. In a matrix form, one has $\mathbf{u_{m1,1}} = \mathbf{a}_1^{-1} \mathbf{u_{b1}}$ where $\mathbf{u}_{\mathbf{m1,1}}^{\mathbf{T}} = \left\langle v_T \quad v_{,xT} \quad v_B \quad v_{,xB} \right\rangle_1$, and $\mathbf{u}_{\mathbf{b1}}^{\mathbf{T}} = \left\langle v \quad \theta \quad v_{,x} \quad \theta_{,x} \right\rangle_1$. By solving for $\mathbf{u_{b1}}$, one has

$$\mathbf{u_{b1}} = \mathbf{a}_1 \mathbf{u_{m1,1}}, \quad \mathbf{a_1} = \frac{1}{2h}\begin{bmatrix} h & 0 & h & 0 \\ -2 & 0 & 2 & 0 \\ 0 & h & 0 & h \\ 0 & -2 & 0 & 2 \end{bmatrix} \tag{24a-b}$$

A similar equation can be written for the second node $\mathbf{u_{b2}} = \mathbf{a}_1 \mathbf{u_{m1,2}}$ where $\mathbf{u}^{\mathbf{T}}_{\mathbf{m1,2}} = \langle v_T \quad v_{,xT} \quad v_B \quad v_{,xB} \rangle_2$, $\mathbf{u}^{\mathbf{T}}_{\mathbf{b}2} = \langle v \quad \theta \quad v_{,x} \quad \theta_{,x} \rangle_2$. Hence, one rewrites in a matrix form

$$\mathbf{u_b} = \begin{Bmatrix} \mathbf{u_{b1}} \\ \mathbf{u_{b2}} \end{Bmatrix} = \mathbf{A}_1 \begin{Bmatrix} \mathbf{u_{m1,1}} \\ \mathbf{u_{m1,2}} \end{Bmatrix} = \begin{bmatrix} \mathbf{a}_1 & \mathbf{0} \\ \mathbf{0} & \mathbf{a}_1 \end{bmatrix} \begin{Bmatrix} \mathbf{u_{m1,1}} \\ \mathbf{u_{m1,2}} \end{Bmatrix}.$$

Cases 2 and 3:

A similar treatment leads to the following expressions for BG1 and BG2 elements

$$\mathbf{A}_2 = \begin{bmatrix} \mathbf{I} & \mathbf{0} \\ \mathbf{0} & \mathbf{a}_1 \end{bmatrix}, \ \mathbf{A}_3 = \begin{bmatrix} \mathbf{a}_1 & \mathbf{0} \\ \mathbf{0} & \mathbf{I} \end{bmatrix} \tag{25a-b}$$

Fig. 7. a) Various type of BG elements, b) buckling kinematics, c) Buckling degrees of freedom

Distortional effects on LTB of simply supported beam

A simply supported beam with W410x39 cross section ($h = 399$, $b = 140, t = 8.8, t_w = 6.4$ mm) and span $L = 8.00m$ is subjected to a point load located at $0.6L$ acting at the shear center. The modulus of elasticity is $E = 200GPa$ and shear modulus is $G = 76.9GPa$. Four bracing scenarios are investigated at the section of the point load; 1) both flanges, 2) only the top flange, 3) only the bottom flange, and 4) no bracing. The critical loads are determined based on 3D shell model under Abaqus, the present distortional (D) and non-distortional modified BG formulations. In the non-distortional solution, the lateral-torsional simply supported end conditions were enforced by restraining the lateral displacement and the angle of twist at both ends. For the distortional and shell solutions, analogous simply supported conditions were achieved by restraining the lateral displacements at the flange-to-web junctions. In the the non-distortional solution, the warping

352 degree of freedom was released at both ends. Correspondingly, in the distortional model, end
353 section global warping was allowed by setting free the weak axis rotations at both flanges. Also,
354 flange local warping was set free by releasing the derivative of the angle of twist at both flanges.
355 Analogous end conditions were adopted in the shell finite model by releasing the longitudinal
356 displacement and the three rotations at all flange nodes offset from the flange-to-web junctions.
357 In the Abaqus model, the S4R shell element was used to mesh the beam. The S4R is a 4-node,
358 quadrilateral shell element with 6 degrees of freedom per node and reduced integration.
359 The beam is meshed using 160 elements along the span, 8 elements across the height, and 4
360 elements to model the flanges. In order to suppress localized buckling of the web under the applied
361 point load, half of the transverse load P is assigned to each of the web-to-flange junctions. Ten
362 elements were found enough to attain convergence in the distortional model. In a similar manner,
363 8 elements were found enough to attain convergence in the modified BG element. In comparison
364 to the 3D FEA predictions, the present distortional (D) model over-predicts the critical moments
365 by 3-4% (Table 1) while the modified BG model over-predicts the critical moments by 6-7%. For
366 the case of no bracing, the ratio of the critical moment as predicted by the modified BG solution
367 to that of the AISC (ANSI/AISC 360-16 (2016)) equation (also based on a non-distortional model)
368 is 1.01%. The results indicate that for a simply supported beam, a typical rolled section (e. g., the
369 W410x39 investigated in this example), distortional effects play a minor role on the magnitude of
370 the critical moments predicted. In such situations, the modified BG formulation, as well as the
371 present non-distortional lateral torsional buckling provisions in design standards tend to slightly
372 overestimate the predicted critical moments. As will be shown in the following section, this
373 observation is non-universal and the influence of web distortion on critical moments varies
374 depending on the boundary conditions, bracing scenarios, cross-sectional geometry, and span.

Table 1. Comparison of critical loads for various bracing scenarios (simply supported beam)

Lateral Torsional Buckling of Gerber beams

Possible bracing scenarios at the cantilever tip include (1) no bracing (denoted as NO in Fig. 8d), (2) top and bottom bracing (TB), (3) only top bracing (T), and (4) only bottom bracing (B). The series of point loads arising from the actions of the OWSJ can be idealized by a uniformly distributed load q acting on the back-span and overhangs. Intermediate OWSJ between columns and between cantilever tip and columns are assumed to provide no lateral restraint to the Gerber beam. This will be the case as long as no additional inclined horizontal braces frame at the OWSJ-beam junction. Assuming a modular system with constant spans L_2 between columns and cantilever spans L_1 , the suspended span is $L_2 - 2L_1$ (**Fig. 8**b) and the corresponding reactions P acting on the tip of the Gerber system (**Fig. 8**c) are also

$$P = q\left(L_2 - 2L_1\right)/2 \tag{26}$$

A system with a back-span $L_2 = 8.00m$ and overhangs $L_1 = 1.50m$ with a W410x39 cross-section is considered as a reference configuration. It is required to obtain the critical moments and associated mode shapes. Three types of solutions are sought: (1) the modified BG non-distortional solution, (2) the distortional solution (D) developed in the present study, and (3) a shell 3D FEA in based on the commercial software Abaqus (SIMULIA (2011)).

Description of the models

In the distortional model, 15 elements were found enough to attain convergence. However, the beam was subdivided into 220 elements to match the discretization of shell model, and thus facilitate the mode shapes comparisons between both models. Also, 10 elements were found enough to attain convergence for the BG solution though the beam was also modelled using 220 elements. At the location of lateral restrains at the flanges, BG1 type elements were used to provide

natural means to model the restraints. The required number of DOFs for convergence using the shell model is 22,542 DOFs. This contrasts with 128 DOFs required in the distortional model and 44 DOFs in the non-distortional BG model.

Results

The critical moments based on the BG element, the distortional element (D) and the 3D shell FEA show that the BG provides the highest capacity, followed by the present distortional element prediction, while the shell solution based on Abaqus provides the lowest capacity (Table 2).

Fig. 8. a) Gerber system, b) suspended span, c) back-span and overhang beams, d) boundary conditions at tips of the overhang e) geometric dimensions of the cross section

Compared to the 3D FEA results, the BG predictions overestimate the critical moments by 11%, 9%, 11%, and 11%, respectively for the cases of no lateral bracing, top flange bracing, bottom flange bracing, and both flanges bracing. In contrast, the present distortional model predictions are only 5% higher than shell FEA predictions for all bracing scenarios. In contrast to the case of simply supported beam, the results show the importance of incorporating distortional effects in the present problem. Such effects are captured in the 3D FEA shell analysis and the present distortional solution, and hence the proximity of their predictions, but not in the conventional non-distortional solution forming the basis of the BG-type element(s). Also, of interest is to note the drastic effect of tip bracing, where restraining both flanges laterally increased the critical moment predictions by over 150% according to all three models. A comparison of mode shapes as characterized by the lateral displacements at the top and bottom flanges u_T and u_B, and the angles of twist θ_T and θ_B (Fig. 9a-c) are in nearly perfect agreement in all three solutions.

Table 2. Comparison of the critical moments

Fig. 9. a) Lateral displacements of the case (NO), b) lateral displacements of the case (TB), c) angle of twist of the case (NO), d) angle of twist for the case (TB)

Parametric study:

In order to study the effects of geometric parameters; flange width b and thickness t, web height h and thickness t_w (all shown in **Fig. 8**e), and spans L_1, L_2 on the critical moment, five dimensionless geometric ratios b/t , h/t_w , b/h , L_2/h and L_2/L_1 are investigated. The beam geometry is taken identical to that defined as a reference case in previous section. The beam has the following dimensionless ratios $b/t = 15.91$, $h/t_w = 60.97$, $b/h = 0.36$, $L_2/h = 20.50$, and $L_2/L_1 = 5.33$. A parametric study is conducted by keeping four of the above five ratios constant, and varying the remaining parameter within the ranges of common sections in the Handbook of Steel Construction (2016). In the first set of runs, the back-span to overhang ratio L_2/L_1 is varied by changing the overhang span L_1 in the ranges of Column 1 in Table 3 while keeping the ratios (b/t , h/t_w , b/h, and L_2/h) identical to those of the reference case. Secondly, the flange width-thickness ratio b/t is varied by changing the flange thickness t according to the values in Column 2 of Table 3 while keeping other ratios (h/t_w , b/h , L_2/h and L_2/L_1) identical to those of the reference case. Next, the web height-thickness ratio h/t_w is varied by changing the web thickness t_w according to Column 3 in Table 3 while keeping other ratios constant. In the fourth set of runs, the flange width-web height b/h is varied by keeping the web height constant while varying the flange width b (Column 4), flange thickness t (Column 2) to preserve the width-thickness ratio b/t identical to that of the reference case. Lastly, the back-span to web height ratio L_2/h was varied

441 by varying the height h and varying b, t and t_w in the ranges of Table 3 to keep the ratios b/t,

442 h/t_w, and b/h equal to those of the reference case.

443 **Table 3.** Geometric parameters ranges

444 The critical moments M_{BG-x} based on the BG model and M_{D-x} based on the distortional model

445 are sought for various bracing scenarios x at the cantilever tips, where x takes the values

446 NO,TB,T,B to respectively denote the cases of no bracing, top and bottom bracings, only top

447 bracing, and only bottom bracing (**Fig. 8**d). Most structural steel design standards (CAN-

448 CSA S16-16 (2016), ANSI/AISC 360-16 (2016), AS-4100 (1998), and EN-1993-1-1-0 2005)

449 define the critical moment as $M_{cr} = C_b M_u$ where C_b is the moment gradient factor and M_u is the

450 elastic critical moment calculated for the case of uniform moments as given by

451 $$M_u = \pi/L\sqrt{EI_y GJ + \left(\pi E/L\right)^2 I_y C_w} \tag{27}$$

452 in which span L is the distance between the points of lateral and torsional restraints. For a given

453 moment distribution, standards provide expressions for C_b for simple boundary conditions which

454 enable the designer to estimate the critical moments. The present models enable the direct

455 computation of the critical moments M_{cr-BG} (based on the non-distortional model) and M_{cr-D}

456 (based on the distortional moment) for the Gerber system. The critical moments computed are then

457 divided by the uniform moment as computed by (27) (by taking the span $L = L_2$ as a reference

458 span) to back-calculate moment gradients C_{b-BG} or C_{b-D}, from the equations

459 $$M_{cr-BG} = C_{b-BG} M_u, \qquad M_{cr-D} = C_{b-D} M_u \tag{28}a-b$$

460 where C_{b-BG} is a moment gradient factor that omits distortional effects and C_{b-D} is a moment

461 gradient factor that incorporates distortion, and the ratio $D = C_{b-D}/C_{b-BG}$ can be thought of as a

462 coefficient that quantifies the effect of distortion on the critical moment. Fig. 10 and Fig. 11a-d
463 depict both moment gradient factors for all four boundary conditions considered.
464 The cantilever span is varied from $L_1 = 900mm$ to $L_1 = 2000mm$ (corresponding to $L_2 / L_1 = 8.89$
465 to $L_2 / L_1 = 4.00$) while the tip loads P were determined according to Eq. (26). The moment
466 gradient factors as determined from Eqs. (28)a-b versus the span ratio L_2/L_1 are depicted in Fig.
467 10 . As expected, the case of no bracing (NO) corresponds to the lowest moment gradient factor
468 and the addition of a top bracing (T) or bottom bracing (B) is found to increase the moment gradient
469 compared to the case of no bracing. In all cases, for a given bracing scenario and span ratio L_2/L_1
470 , the distortional moment gradient is consistently lower than the non-distortional moment gradient.
471 This is a natural outcome of the fact that the distortional model provides a more flexible
472 representation of the section deformation than the BG type solution where the section is assumed
473 to displace and twist as a rigid disk.
474 The distortional model shows that top bracing increases the moment gradient C_{b-D} by factor of
475 116% to 168% which is comparable to the increase of 116 % to 167% a. predicted by the non-
476 distortional moment gradient C_{b-BG} . As a general observation, top bracing becomes less effective
477 as the cantilever span decreases (i.e., L_2/L_1 increases). Bottom bracing is found ineffective as it
478 increases the moment gradient moment distortional by a factor not exceeding 103% based
479 distortional and non-distortional models. In contrast, top and bottom flanges bracing (TB)
480 significantly increases the moment gradient factor compared to the case of no bracing. The increase
481 predicted by the distortional model ranges from 142% to 180% while that predicted by the non-
482 distortional model ranges from 149% to 185%.

The effects of b/t, h/t_w, b/h, L_2/h on the moment gradients C_{b-BG} and C_{b-D} are depicted on Fig. 11a-d. In general, when both flanges are braced (TB), the moment gradient factor C_{b-BG} based on the non-distortional model are found insensitive to b/t, h/t_w, b/h, L_2/h as observed by the flat curves on Fig. 11a-d. In contrast, the moment gradient factor C_{b-D} based on the distortional model shows a positive trend with b/t and L_2/h and a negative trend with h/t_w and b/h. For the other three bracing scenarios (B, T, NO), the moment gradient factors C_{b-BG} and C_{b-D} reduce with b/t, h/t_w and b/h, and increase with L_2/h .

The effect of distortion as characterized by the ratio of the moment gradients C_{b-D}/C_{b-BG} is observed to be most pronounced for top and bottom flanges bracing (TB). This is evidenced by the consistently lower C_{b-D}/C_{b-BG} ratio relative to those based on other bracing scenarios (T, B, and NO). Figure 11a indicated that TB bracing distortional effects are insensitive to the flange slenderness since the C_{b-D}/C_{b-BG} ratio varies within the narrow range of 0.92-0.94 when $b/t = 9.3 - 23.3$. In contrast, Figures 11b-c suggest that distortional effects are sensitive for the web slenderness h/t_w and the cross-section aspect ratio b/h. In Fig. 11b, ratio C_{b-D}/C_{b-BG} is found to vary from 0.86 (at $h/t_w = 97.6$) to 0.98 (at $h/t_w = 39.0$) and in Fig. 11c, it varies from 0.79 (at $b/h = 0.64$) to 0.96 (at $b/h = 0.31$). Figure 11d shows that distortion is sensitive to the span to depth ratio L_2/h as C_{b-D}/C_{b-BG} varies from 0.83 (at $L_2/h = 13.3$) to 0.97 at ($L_2/h = 26.7$) .

For the case of no bracing (NO), distortion is found to be only mildly sensitive to changes in b/t, h/t_w, b/h, and L_2/h, as the C_{b-D}/C_{b-BG} ratio is found to vary within a relatively narrow ranges: from 0.94 (at $b/t = 9.3$) to 0.98 at ($b/t = 23.3$) in Fig. 11a, from 0.92 (at $h/t_w = 97.6$) to 0.99 (at

503 $h/t_w = 39.0$) in Fig. 11b, from 0.87 (at $b/h = 0.64$) to 0.98 (at $b/h = 0.31$) in Fig. 11c, and from

504 0.93 (at $L_2/h = 13.3$) to 0.99 (at $L_2/h = 26.7$) in Fig. 11d. The distortional effects for top flange

505 bracing (T) and bottom flange bracing (B) are observed to lie between the cases of both flange

506 bracing (TB) and no bracing (NO).

507 For top flange bracing (T) and for bottom flange bracing (B), ratios C_{b-D}/C_{b-BG} were essentially

508 identical to the those of the case of no bracing (NO) in all cases, suggesting that the degree of

509 distortion in the T and B bracing is comparable to that of the no bracing.

510 **Fig. 10.** Moment gradient factor versus back span to overhang ratio L_2/L_1

511

512 **Fig. 11.** Moment gradient factors versus (a) flange width to thickness ratio b/t, b) web height to

513 thickness ratio h/t_w, (b) flange width to web height ratio b/h, and (d) back span to web height

514 ratio L_2/h, (all vertical lines correspond to the reference case)

515 ## Summary and Conclusions

516 1) The present study modified the distortional finite element formulation by Bradford and Trahair

517 (1982) to model doubly symmetric wide flange sections, account for flange local warping, account

518 for load height destabilizing effect, and account for the parabolic distribution of the shear stresses

519 along the web height. The formulation treats the web as a thin plate and thus captures web

520 distortion within the plane of the cross-section and treats both flanges as Gjelsvik members with

521 unequal angles of twist and lateral displacement fields. Modifications are also made to the

522 conventional non-distortional lateral torsional buckling finite element of Barsoum and Gallagher

523 (1970) to enable the analyst to model the lateral braces at either of the two flanges, while preserving

524 the positive definite nature of the resulting stiffness matrix.

2) In all examples investigated, the lowest critical moments predicted were obtained by the shell finite element solution, closely followed by the present distortional solution, and the highest critical moments were obtained by the non-distortional solution.

3) For the simply supported beam investigated, the distortional solution is found to predict critical moments in close agreement with those predicted by the shell finite element solution while the non-distortional finite element solution slightly overestimates the critical moments as predicted by Abaqus, but in very close agreement to the present ANSI/AISC 360-16 (2016) predictions. The results suggest that the conventional non-distortional model adequately predicts the critical moment for the problem, albeit it errs on the un-conservative side.

4) The distortional and non-distortional models were used to a develop moment gradient factors for the Gerber system in a parametric study. The ratio of the non-distortional to distortional moment gradients is indicative of the influence of distortion on the predicted critical moments.

5) The following observations based on the parametric study can be of practical interest when engineering Gerber beam systems:

i. In general, the conventional non-distortional model grossly overestimates the critical moment compared to the distortional model. As such, it is recommended to adopt a distortional solution when determining the capacity of Gerber systems.

ii. Bracing both flanges laterally at the tips of the cantilever span is found to be particularly effective in increasing the critical moments compared to the case of no lateral bracing at the tip. In comparison, top flange bracing is found moderately effective.

iii. For a given Gerber beam, distortional effects tend to be most significant when the tips of both flanges are laterally braced.

iv. For a given span ratio L_2/L_1 , distortional effects tend to increase (i.e., C_{b-D}/C_{b-BG} tend to decrease) with the web slenderness ratio h/t_w and the section aspect ratio b/h . Also, distortional effects significantly decrease with the span to depth ratio (h/L_2) and mildly decrease with the flange to thickness ratio b/t .

Acknowledgements

The authors wish to express their gratitude to Mr. George Casoli, Dr. Feng Rong, Dr. Siriwut Sasibut, and Dr. Marinos Stylianou, from S-FRAME Software Inc. for their feedback throughout the project. Financial support from S-FRAME Software Inc. and matching funds from the Natural Sciences and Engineering Research Council (NSERC) of Canada are also gratefully acknowledged.

References

ANSI/AISC 360-16 (2016). "ANSI/AISC 360-16." *Specification for structural steel buildings*, American Institute of Steel Construction (AISC), Chicago, IL.

AS-4100 (1998). "AS 4100 steel structures."Sydney, Australia.

AS/NZS 4600-05 (2005). "AS/NZS 4600 Cold Formed Steel Structures." Standards Australia (SA), Sydney, Australia. .

Barsoum, R. S., and Gallagher, R. H. (1970). "Finite element analysis of torsional and torsional–flexural stability problems." *International Journal for Numerical Methods in Engineering*, 2(3), 335-352.

Basaglia, C., and Camotim, D. (2013). "Enhanced generalised beam theory buckling formulation to handle transverse load application effects." *International Journal of Solids and Structures*, 50(3–4), 531-547.

Bradford, M. A., and Trahair, N. S. (1981). "Distortional Buckling of I-Beams." *Journal of the Structural Division, ASCE*, 107(2), 355-370.

Bradford, M. A., and Trahair, N. S. (1982). "Distortional buckling of thin-web beam-columns." *Engineering Structures*, 4(1), 2-10.

Bradford Mark, A., and Trahair Nicholas, S. (1983). "Lateral Stability of Beams on Seats." *Journal of Structural Engineering*, 109(9), 2212-2215.

CAN-CSA S16-16 (2016). "Handbook of Steel Construction." *CSA-S16-16 Specification*, Canadian Institute of Steel Construction, CA.

Chin, C. K., Al-Bermani, F. G. A., and Kitipornchai, S. (1992). "Stability of thin-walled members having arbitrary flange shape and flexible web." *Engineering Structures*, 14(2), 121-132.

CISC-ICCA (2016). "Handbook of Steel Construction." Canadian Institute of Steel Construction, CA.

de Miranda, S., Gutiérrez, A., Miletta, R., and Ubertini, F. (2013). "A generalized beam theory with shear deformation." *Thin-Walled Structures*, 67(0), 88-100.

Dekker, N. W., and Kemp, A. R. (1998). "A simplified distortional buckling model for doubly symmetrical I-sections." *Canadian Journal of Civil Engineering*, 25(4), 718-727.

EN-1993-1-1-05 (2005). "Eurocode 3: Design of Steel Structures-General Rules and Rules for Buildings." European Committee of Standardization (CEN), Brussels, Belgium.

Erkmen, R. E., and Mohareb, M. (2006a). "Nonorthogonal solution for thin-walled members – a finite element formulation." *Canadian Journal of Civil Engineering*, 33(4), 421-439.

Erkmen, R. E., and Mohareb, M. (2006b). "Nonorthogonal solution for thin-walled members – applications and modelling considerations." *Canadian Journal of Civil Engineering*, 33(4), 440-450.

Gjelsvik, A. (1981). *The theory of thin walled bars / Atle Gjelsvik*, Wiley, New York, NY, USA.

Hancock, G. J. (1978). "Local, Distortional, and Lateral Buckling of I-Beams." *Journal of the Structural Division*, 104(11), 1787-1798.

Hancock, G. J., Bradford, M. A., and Trahair, N. S. (1980). "Web distortion and flexural-torsional buckling." *Journal of the Structural Division, ASCE*, 106(7), 1557-1571.

Hassan, R., and Mohareb, M. (2015). "Distortional lateral torsional buckling for simply supported beams with web cleats." *Canadian Journal of Civil Engineering*, 42(12), 1091-1103.

Hughes, O., and Ma, M. (1996a). "Lateral Distortional Buckling of Monosymmetric Beams under Point Load." *Journal of Engineering Mechanics*, 122(10), 1022-1029.

Kumar, A., and Samanta, A. (2006b). "Distortional buckling in monosymmetric I-beams: Reverse-curvature bending." *Thin-Walled Structures*, 44(7), 721-725.

Ma, M., and Hughes, O. (1996b). "Lateral distortional buckling of monosymmetric I-beams under distributed vertical load." *Thin-Walled Structures*, 26(2), 123-145.

Ng, M. L.-H., and Ronagh, H. R. (2004). "An Analytical Solution for the Elastic Lateral-Distortional Buckling of I-section Beams." *Advances in Structural Engineering*, 7(2), 189-200

Pezeshky, P., and Mohareb, M. (2014). "Distortional theory for the analysis of wide flange steel beams." *Engineering Structures*, 75, 181-196.

Pezeshky, P., and Mohareb, M. (2015). "Finite-Element Formulations for the Distortional Analysis of Wide Flange Steel Beams." *Journal of Engineering Mechanics*, 04015071.

Pezeshky, P., Sahraei, A., and Mohareb, M. (2017). "Effect of bracing heights on lateral torsional buckling resistance of steel beams." *CSCE, The 6th International Conference on Engineering Mechanics and Materials.* Vancouver, BC.

Pi, Y., and Trahair, N. (2000). "Distortion and Warping at Beam Supports." *Journal of Structural Engineering*, 126(11), 1279-1287.

Sahraei, A., and Mohareb, M. (2016). "Upper and lower bound solutions for lateral-torsional buckling of doubly symmetric members." *Thin-Walled Structures*, 102, 180-196.

Sahraei, A., and Mohareb, M. (2016). "Upper and lower bound solutions for lateral-torsional buckling of doubly symmetric members." *Thin-Walled Structures*, 102(Supplement C), 180-196.

Sahraei, A., Pezeshky, P., Mohareb, M., and Doudak, G. (2018). "Simplified Expressions for Elastic Lateral Torsional Buckling of Wooden Beams." *Engineering Structures*, In press.

624 Samanta, A., and Kumar, A. (2006a). "Distortional buckling in monosymmetric I-beams." *Thin-*
625 *Walled Structures*, 44(1), 51-56.
626 Samanta, A., and Kumar, A. (2008). "Distortional buckling in braced-cantilever I-beams." *Thin-*
627 *Walled Structures*, 46(6), 637-645.
628 SIMULIA. 2011. Abaqus/CAE Analysis, version 6.11-1Dassault Systemes.
629 Timoshenko, S., and Woinowsky-Krieger, S. (1956). *Theory of plates and shells*, McGraw-Hill,
630 Inc.
631 Trahair, N. S. (1993). *Flexural-torsional buckling of structures*, CRC Press, USA.
632 Vieira, R. F., Virtuoso, F. B. E., and Pereira, E. B. R. (2017). "Buckling of thin-walled structures
633 through a higher order beam model." *Computers & Structures*, 180, 104-116.
634 Wang, C. M., Chin, C. K., and Kitipornchai, S. (1991). "Parametric study on distortional buckling
635 of monosymmetric beam-columns." *Journal of Constructional Steel Research*, 18(2), 89-
636 110.
637 Wu, L., and Mohareb, M. (2011a). "Buckling of shear deformable thin-walled members--I.
638 Variational principle and analyticalsolutions." *Thin-Walled Structures*, 49(1), 197-207.
639 Wu, L., and Mohareb, M. (2011b). "Buckling of shear deformable thin-walled members--II. Finite
640 Element Formulation." *Thin-Walled Structures*, 49(1), 208-222.
641 Zirakian, T., and Showkati, H. (2006). "Distortional buckling of castellated beams." *Journal of*
642 *Constructional Steel Research*, 62(9), 863-871.
643 Zirakian, T., and Showkati, H. (2007). "Experiments on Distortional Buckling of I-Beams."
644 *Journal of Structural Engineering*, 133(7), 1009-1017.
645
646

Table 1. Comparison of critical loads for various bracing scenarios (simply supported beam)

Bracing Location	Critical load (kN)			Ratio	
	Shell 3D FEA	Distortional D	Non-Distortional BG	D/FEA	BG/FEA
Top Flange	99.7	104.1	106.4	1.04	1.07
Bottom Flange	28.6	29.4	30.5	1.03	1.07
Both Flanges	100.4	104.9	107.1	1.04	1.07
No Bracing	26.2	27.1	27.8	1.03	1.06

Table 2. Comparison of the critical moments

Lateral bracing at overhang tips	Critical moments (kNm)			Ratios	
	BG	D	FEA*	BG/FEA	D/FEA
No bracing	44.7	42.3	40.17	1.11	1.05
Top Flange	59.9	57.9	55.0	1.09	1.05
Bottom Flange	44.7	42.4	40.2	1.11	1.05
Top and Bottom	70.43	65.9	63.5	1.11	1.04

*FEA based on the 3D FEA Abaqus model

Table 3. Geometric parameters ranges

(1) span L_1 (mm)	(2) Flange thickness t (mm)	(3) Web thickness t_w (mm)	(4) Flange Width b (mm)	(5) Section height h (mm)
900	6	4.0	120	200
1000	6.5	4.5	130	250
1200	7	5.0	140	300
1300	8	5.5	150	350
1400	8.8	6.0	170	390.2
1500	10	6.4	180	450
1600	11	7.0	190	500
1700	12	7.5	200	550
1800	13	8.0	210	600
1900	14	9.0	230	650
2000	15	10.0	250	700

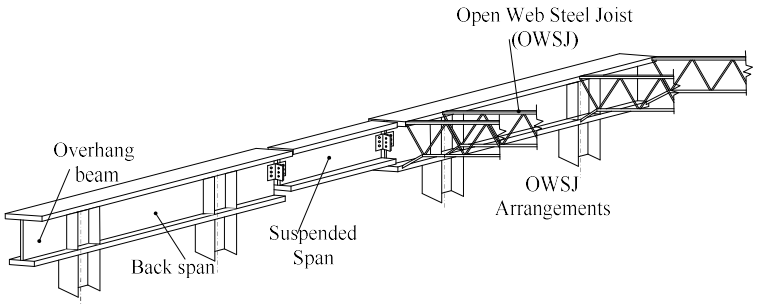

Fig. 12. Gerber beam system

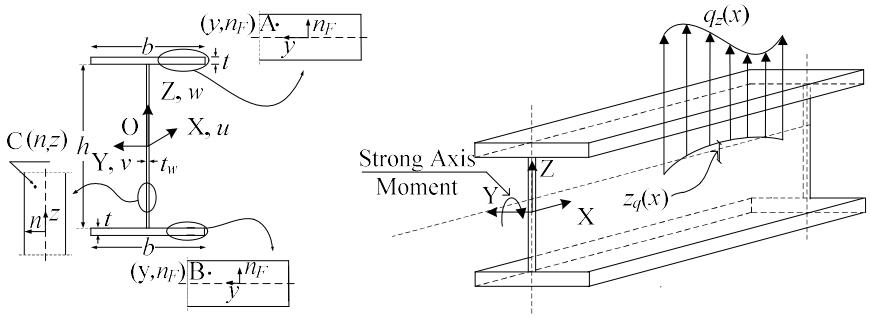

(a) (b)

Fig. 13. a) Cross section geometry b) general type of loads

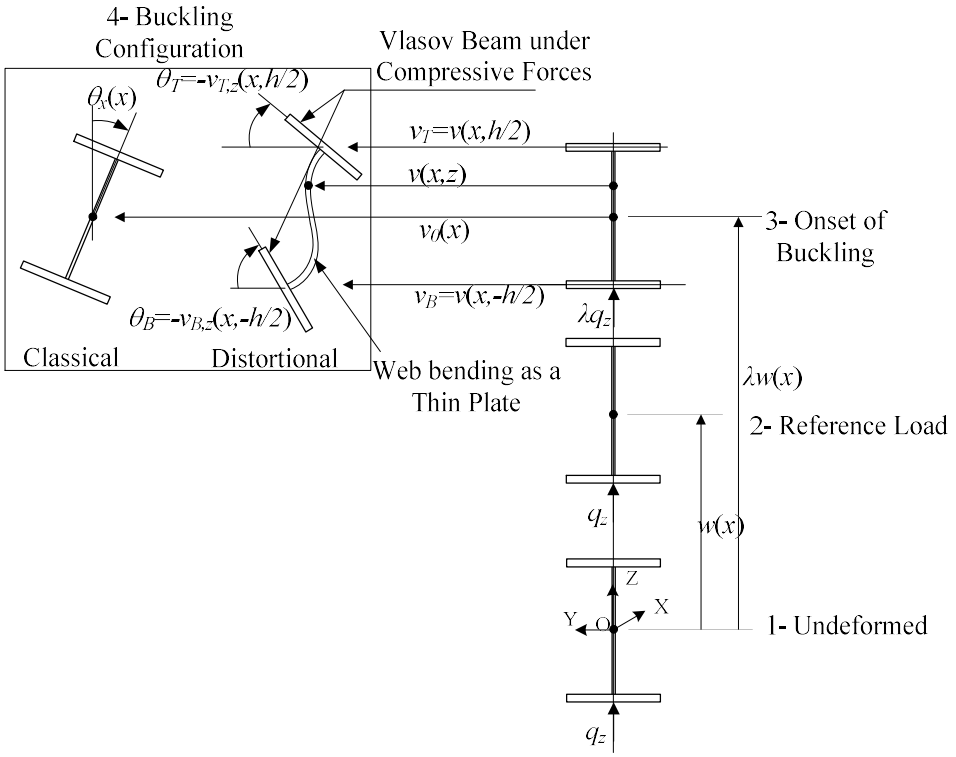

Fig. 14. Deformation stages of buckling

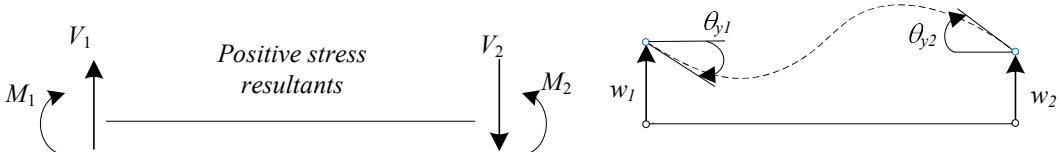

Fig. 15. Sign convention for stress resultants

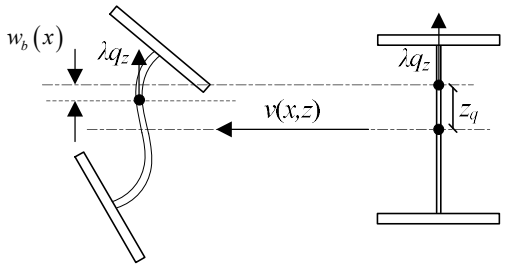

665
666 **Fig. 16.** Vertical distance travelled by load throughout buckling

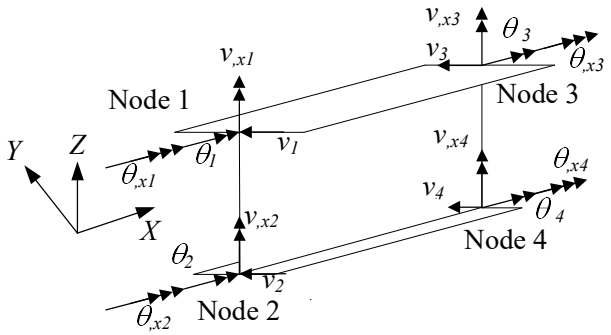

667
668 **Fig. 17.** Definition of the 16 DOFs in the distortional buckling element

669

670

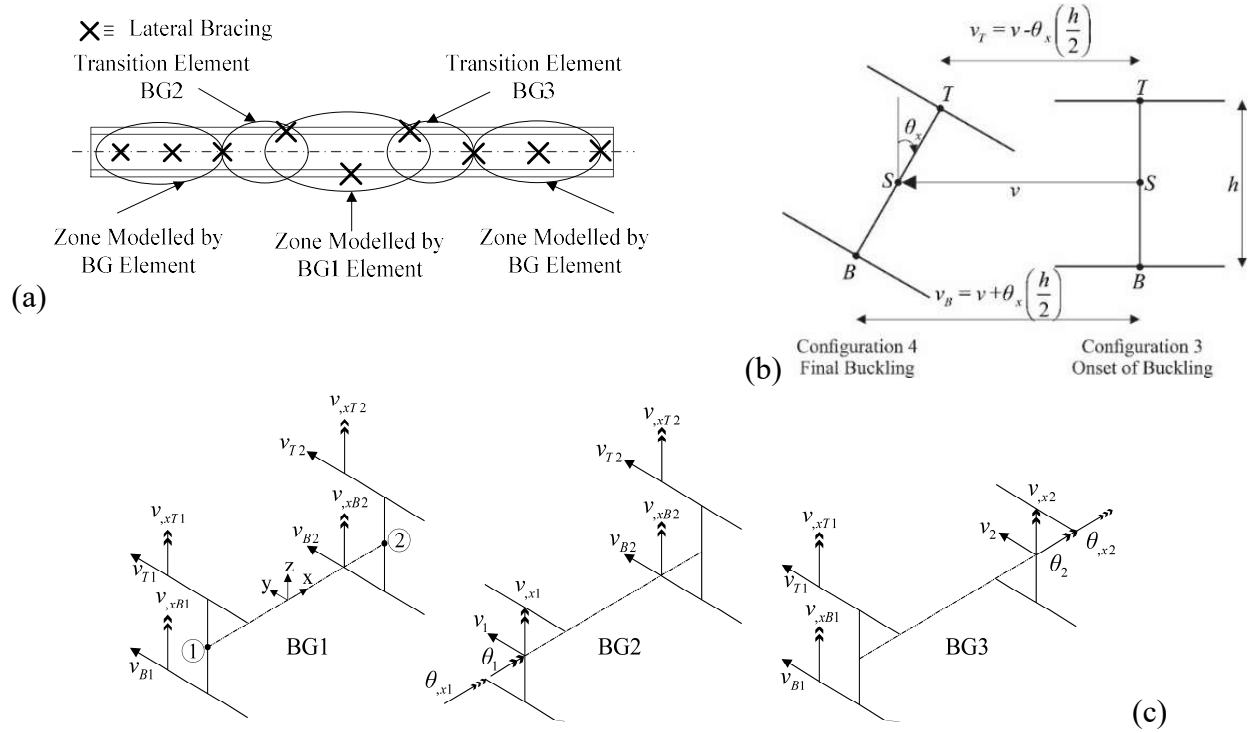

671 **Fig. 18.** a) Various type of BG elements, b) buckling kinematics, c) Buckling degrees of freedom

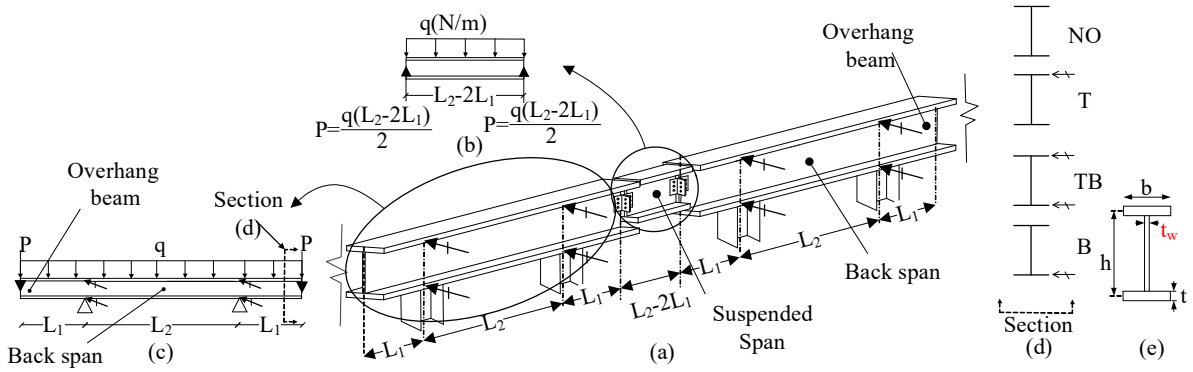

672
673 **Fig. 19.** a) Gerber system, b) suspended span, c) back-span and overhang beams, d) boundary
674 conditions at tips of the overhang e) geometric dimensions of the cross section
675
676

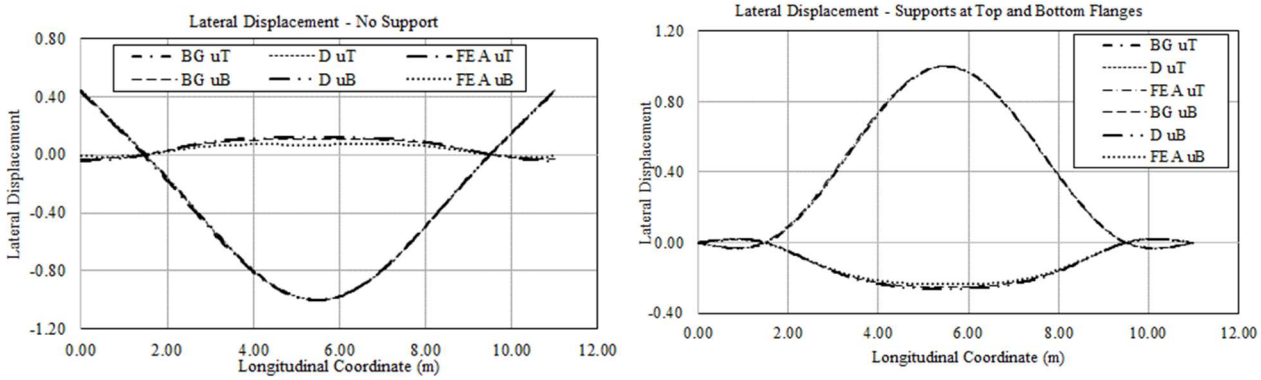

677

678 (a) (b)

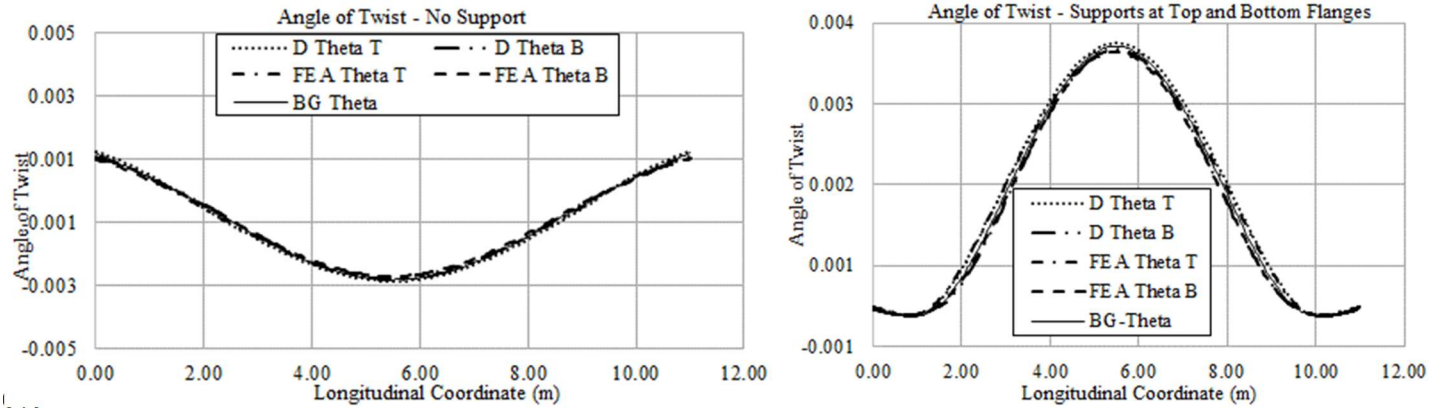

680 (c) (d)

681 **Fig. 20.** a) Lateral displacements of the case (NO), b) lateral displacements of the case (TB), c)
682 angle of twist of the case (NO), d) angle of twist for the case (TB)
683

684

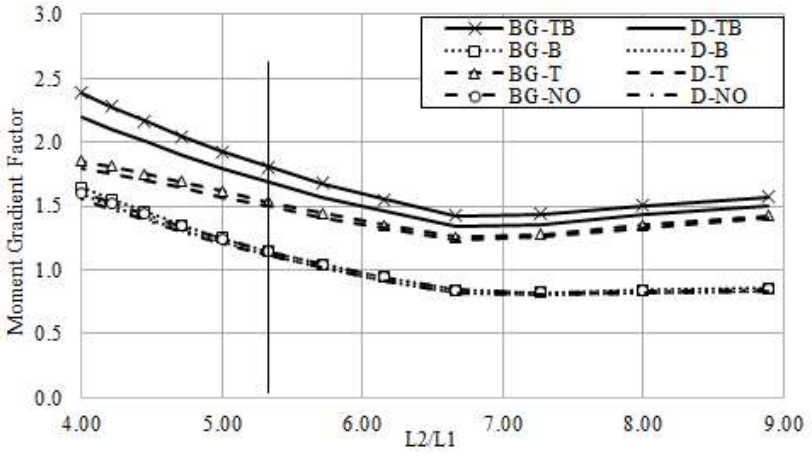

685
686 **Fig. 21.** Moment gradient factor versus back span to overhang ratio L_2/L_1

687
688

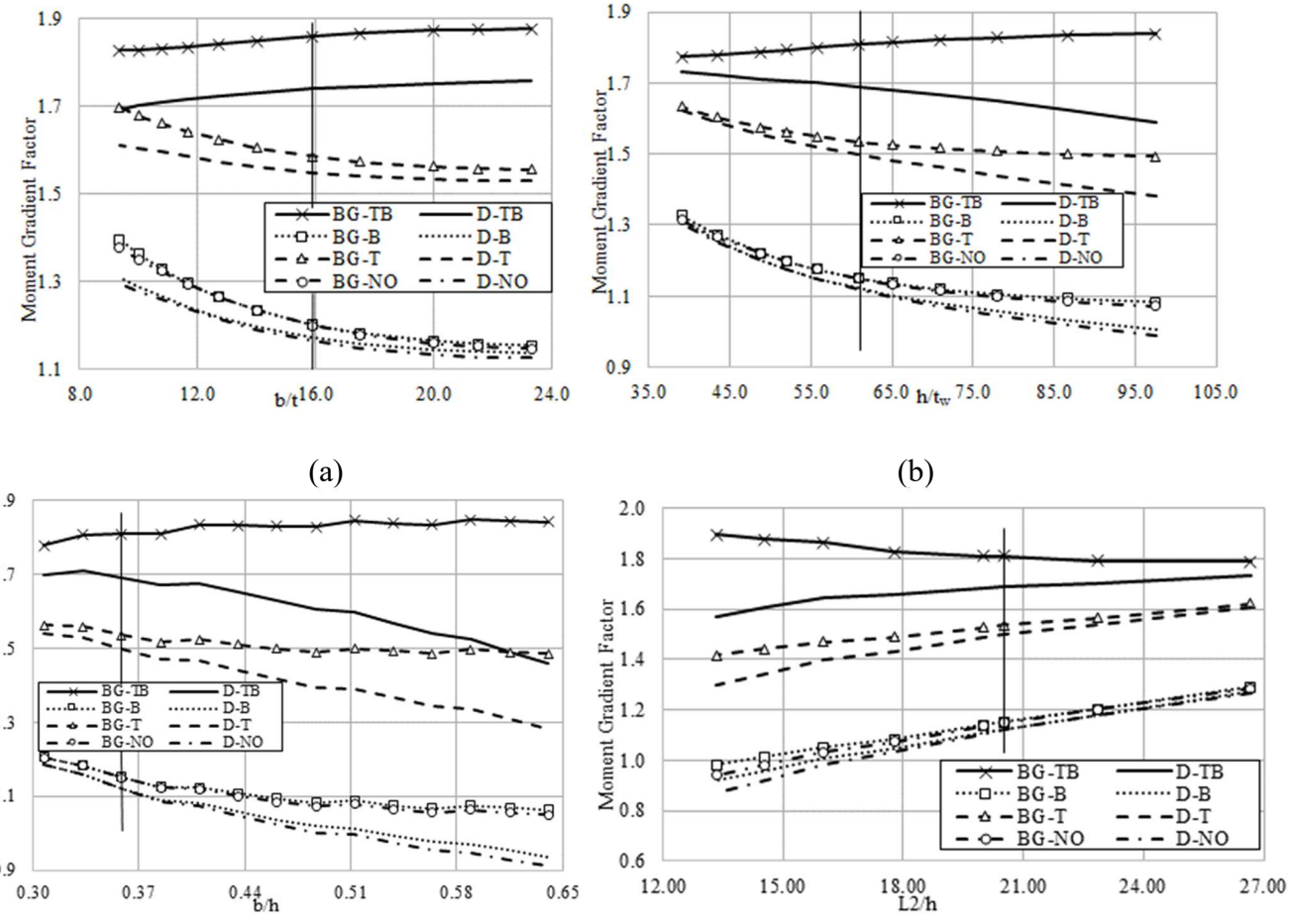

689
690
691
692
693
694 **Fig. 22.** Moment gradient factors versus (a) flange width to thickness ratio b/t, b) web height to
695 thickness ratio h/t_w, (b) flange width to web height ratio b/h, and (d) back span to web height
696 ratio L_2/h, (all vertical lines correspond to the reference case)
697